Effects of first-order spatial dispersion on phonon focusing: Application to quartz

A. G. Every
Department of Physics, University of the Witwatersrand, Johannesburg 2001, South Africa
(Received 25 February 1987)

First-order spatial dispersion has a considerable impact on phonon focusing in the vicinity of the acoustic axes of crystals, even for frequencies well below 1 THz. Subject to certain symmetry requirements, the degeneracy of the transverse sheets of the acoustic slowness surface is removed at finite wave vector and frequency. As a result, the phonon intensity anticaustic associated with a conical degeneracy is transformed into a similarly shaped caustic. Intersecting line caustics associated with a tangential degeneracy at a fourfold axis break apart and form cusps. Lines of wedge-shaped degeneracy in hexagonal crystals are removed, thereby giving rise to pairs of circular caustics. It is shown that a simple treatment of first-order spatial dispersion is well able to explain a number of anomalies in the published phonon images of quartz.

I. INTRODUCTION

There is a great deal of interest at the present time in the ballistic transport and focusing properties[1] of large-wave-vector dispersive phonons in crystals.[2–6] By using superconducting tunnel-junction detectors and taking advantage of the strong frequency dependence of phonon-scattering processes, investigators have had considerable success in obtaining monochromatic high-frequency phonon focusing patterns for crystals such as Ge,[3] GaAs,[4] and InSb.[5] Comparatively little attention has, however, been given to the effects of linear spatial dispersion[7–10] on phonon focusing at lower frequencies. Because of time-reversal invariance, dispersive effects are normally quadratic in $\mathbf{k}$ in leading order, and so only become important at higher frequencies. However, along acoustic axes and subject to certain symmetry requirements, lifting of the transverse mode degeneracy occurs at finite $\mathbf{k}$, resulting in changes to the shape of the acoustic slowness surface which are *linear* in $\mathbf{k}$. These changes in turn have a considerable impact on the phonon focusing pattern of a crystal, even for frequencies well within the regime of conventional phonon imaging based on bolometric detection techniques. Various effects come about, depending on the type of degeneracy. The phonon intensity anticaustic associated with a point of conical degeneracy is transformed at finite k or frequency ν into a similarly shaped caustic. A commonly occurring pattern of intersecting line caustics, associated with the tangential degeneracy at a fourfold axis of symmetry, breaks apart to form a set of four cusps. Lines of wedge-shaped degeneracy in hexagonal crystals are removed, thereby giving rise to pairs of circular caustics.

Linear spatial dispersion derives from the first-order terms in the power-series expansion of the wave-vector-dependent elastic moduli $C_{ijlm}(\mathbf{k})$. The coefficients of these terms constitute the acoustic gyrotropic tensor d_{ijlmn}. In this paper we show that a simple treatment of first-order spatial dispersion, based on a single component of d_{ijlmn}, is well able to resolve a number of anomalies in the published phonon images of quartz.[11,12] We do so by tracing out the evolution of the pattern of phonon focusing caustics with increasing k, and by means of Monte Carlo simulations of the phonon intensity based on the assumption of a Planck distribution of phonons with cutoff at $0.1k_{\mathrm{BZ}}$, where k_{BZ} is the c-axis zone boundary wave vector, and heat source temperature ranging up to 10 K.

II. THE ELASTIC WAVE EQUATION INCORPORATING DISPERSION

The onset of phonon dispersion can conveniently be treated in the context of continuum elasticity theory by expanding the elastic moduli $C_{ijlm}(\mathbf{k})$ in power series in $\mathbf{k}$ and retaining only the leading terms of a low order. In this way one significantly extends the range of applicability of continuum elasticity theory, thereby delaying the stage at which it becomes necessary to cross over to the use of lattice-dynamics models. The advantages of this approach are especially appealing where one is dealing with materials which have complex unit cells and thus a large number of branches to their phonon dispersion relation. Subject to certain symmetry requirements, dispersion in phonon velocities is linear in $\mathbf{k}$ in the vicinity of acoustic axes, and this gives rise to effects which are measurable at frequencies even as low as 1 GHz. At thermal phonon frequencies $\nu \gtrsim 100$ GHz, the effects of linear dispersion can be substantial.

The equations of motion for a dispersive elastic medium admit plane-wave solutions of the form $\mathbf{u}=\mathbf{U}\exp[i(\mathbf{k}\cdot\mathbf{x}-\omega t)]$, which are governed by the Christoffel equations[7,9]

$$(\Gamma_{il}-\rho\omega^2\delta_{il})U_l=0\ , \tag{1}$$

where ρ is the density of the medium and δ_{il} is the δ function. The Christoffel coefficients Γ_{il} may be decomposed into terms comprising successive powers of $\mathbf{k}$, thus

$$\Gamma_{il}=\Gamma_{il}^{(0)}+\Gamma_{il}^{(1)}+\Gamma_{il}^{(2)}+\cdots\ , \tag{2}$$

where

$$\Gamma_{il}^{(0)} = C_{ijlm} k_j k_m \ , \tag{3}$$

and

$$\Gamma_{il}^{(1)} = i d_{ijlmn} k_j k_m k_n \ , \tag{4}$$

etc., where C_{ijlm} are the elastic moduli and d_{ijlmn} is the acoustic gyrotropic tensor. The crystal classes which allow linear dispersion, with the exception of class 432, also permit the piezoelectric effect. Piezoelectric stiffening of the elastic constants[13] is taken into account by setting

$$C_{ijlm} = C_{ijlm}^{E} + \frac{e_{ijr} e_{lms} k_r k_s}{\epsilon_{pq}^{s} k_p k_q} \ , \tag{5}$$

where C_{ijlm}^{E} are the elastic moduli at constant electric field, e_{ijr} is the piezoelectric stress tensor, and ϵ_{pq}^{s} is the permittivity tensor at constant elastic strain. $\Gamma_{il}^{(1)}$ comprises the first-order terms in the expansion of $C_{ijlm}(\mathbf{k})$. Because of time-reversal invariance, $C_{ijlm}(-\mathbf{k}) = C_{lmij}(\mathbf{k})$, from which it follows[7,9] that $d_{ijlmn} = -d_{lmijn}$. Since the stress and strain tensors are symmetric, d_{ijlmn} is symmetric with respect to interchange of i and j and of l and m, and so it can be written in contracted Voigt notation[14] as d_{IJn}. Crystal symmetry restricts the number of independent components of d_{IJn}. In particular, the presence of a center of inversion causes the tensor to vanish identically. Kumaraswamy and Krishnamurthy[15] have listed the nonvanishing components of d_{IJn} for the noncentrosymmetric crystal classes.

The validity of the power-series expansion of elastic constants in $\mathbf{k}$ comes into question where there are long-range interatomic forces at play. These can give rise to nonanalytic terms in $\mathbf{k}$, the fully study of which has not yet been undertaken.[9] DiVincenzo[9] concludes that the effects of nonanalyticity are small for acoustic dispersion, at least in the case of GaAs. The published results on acoustical activity and related phenomena are, moreover, all well accounted for without invoking nonanalytic terms.

For small $\mathbf{k}$, $\Gamma^{(0)} \gg \Gamma^{(1)} \gg \Gamma^{(2)} \gg \cdots$, and so the Christoffel equations may be solved initially by retaining $\Gamma^{(0)}$ only, and then treating $\Gamma^{(1)}$ and $\Gamma^{(2)}$ etc. by perturbation theory. DiVincenzo[9] has shown that when the unperturbed velocities are nondegenerate, $\Gamma^{(1)}$ contributes only in second order while the subsequent term $\Gamma^{(2)} = f_{ijlmnr} k_j k_m k_n k_r$ survives in first order of perturbation. Both terms, as a result, give rise to velocity changes which are quadratic in $\mathbf{k}$. It is to this normal absence of linear dispersion that one can, to a large extent, attribute the success of continuum elasticity theory in successfully accounting for most of the published phonon focusing patterns in which the phonon frequencies range up to ~ 0.5 THz.

This paper is, however, specifically concerned with phonon focusing in the vicinity of acoustic axes (i.e., directions where two or more unperturbed velocities coincide). Here the energy denominators in the second-order perturbation expressions for $\Gamma^{(1)}$ are small and so these terms become large in comparison with the first-order perturbation terms for $\Gamma^{(2)}$. To a good approximation the latter terms may then be neglected. Precisely along an acoustic axis, perturbation theory shows that the degeneracy of the velocities is lifted to first order in $\mathbf{k}$ by the $\Gamma^{(1)}$. For small $\mathbf{k}$, these linear shifts are far greater in magnitude than the quadratic dispersion of $\Gamma^{(2)}$, and they give rise to observable effects even at frequencies on the order of 1 GHz.

The perturbed modes that emerge from the lifting of the degeneracy are, in general, elliptically polarized (circular polarization if $\mathbf{k}$ lies precisely along a direction of threefold or higher symmetry). This gives rise to the phenomenon of acoustical activity (the rotation of the plane of polarization of a plane polarized wave).

First-order spatial dispersion has been studied using a variety of techniques including inelastic neutron scattering,[16,17] Brillouin scattering,[18] acoustical activity,[19,20] acoustic time-of-flight measurements,[21] Bragg reflection of light,[22] and heat pulse techniques,[10] and certain components of their gyrotropic tensors have been experimentally determined for quartz, $NaClO_3$, and $Bi_{12}GeO_{20}$. In addition, on the basis of lattice-dynamics models d_{623} has been calculated for GaAs by DiVincenzo[9] and d_{543} for tellurium by Portigal and Burstein.[7]

For the lower-symmetry classes d_{IJn} tends to have a large number of independent components (a maximum of 30 in the case of triclinic 1). Measurements of acoustical activity, in principal, yield the value of one component or a combination of components of d_{IJn} for each inequivalent acoustic axis. Since the number of isolated acoustic axes that a crystal can have is strictly limited (in the case of orthorhombic media, for instance, Musgrave[23] has shown that there can at most be 16 acoustic axes, many of which belong to equivalent sets), a complete determination of the d_{IJn} tensor from acoustical activity measurements alone is evidently impossible for many of the crystal classes.

Directions of threefold, fourfold, and sixfold symmetry are pure mode directions with the two transverse modes being degenerage in the limit $k \to 0$. Taking the $\mathbf{X}_3$ axis to be along this direction, symmetry consideration[7] shows that for $\mathbf{k} \| \mathbf{X}_3$

$$\Gamma_{23}^{(1)} = \Gamma_{31}^{(1)} = 0 \ , \tag{6}$$

and

$$\Gamma_{12}^{(1)} = -\Gamma_{21}^{(1)} = i d_{13233} k_3^3 = i d_{543} k_3^3 \ . \tag{7}$$

When $\mathbf{k}$ deviates from the X_3 axis, $\Gamma_{23}^{(1)}$ $\Gamma_{31}^{(1)}$, and $\Gamma_{12}^{(1)}$ acquire terms of the form $k_1 k_3^2$, $k_2 k_3^2$, etc. Provided that the angle of deviation is small, these terms can be ignored. The calculations reported in this paper are all based on this approximation.

The secular equation for Eq. (1), retaining only $\Gamma_{il}^{(0)}$ and $\Gamma_{il}^{(1)}$, is

$$| \Gamma_{il}^{(0)} + \Gamma_{il}^{(1)} - \rho \omega^2 \delta_{il} | = 0 \ . \tag{8}$$

On expanding the determinant, one obtains a cubic equation in ω^2 which has real coefficients. The solutions are conveniently expressed in terms of trigonometric functions.[24] The phase velocities for the modes are then given by $v = \omega / k$ and the group velocities $\mathbf{V} = \partial \omega / \partial \mathbf{k}$ are readily obtained by implicit differentiation from the cubic equation. The method that has been used is an extension of

that developed by Every and McCurdy[25] for piezoelectric crystals.

III. PHONON FOCUSING

Phonon focusing is a phenomenon that occurs as a result of the nonspherical shape of phonon constant frequency or slowness surfaces of crystals.[26] Phonon ray vectors $\mathbf{V}=\partial\omega/\partial\mathbf{k}$ are constrained to be normal to their constant frequency surfaces, and so they become bunched up in direction or focused where these surfaces are relatively flat. The degree of focusing or phonon intensity is inversely proportional to the Gaussian curvature of these surfaces[27–29] in the long-wavelength limit or for a monochromatic phonon source. At parabolic lines separating regions of negative and positive Gaussian curvature, the curvature is locally zero and the focusing thus mathematically infinite. This is the origin of the caustics which are a prominent feature of most phonon images.[1] The patterns these caustics form have been extensively investigated by a number of authors.[29–32]

Phonon images display the complex directional dependence of the phonon flux emanating from a localized heat source. They are generated experimentally by raster scanning either the heat source or detector.[12,27,33] Monte-Carlo–simulated images are constructed[27] by taking a smooth distribution of phonon wave vectors and sorting their associated ray vectors in directions to form a polar plot of phonon intensity or a plane projected image.

The existence of dispersion causes the shape of the slowness surfaces to be ω or k dependent, and the phonon focusing patterns and the caustics they contain thus also depend on ω or k. At the opposite extreme to infinite focusing is the infinite defocusing that occurs at points of internal conical refraction where two sheets of a slowness surface meet in the form of a double cone as depicted in Fig. 1(a). The Gaussian curvature diverges at the point of contact, and so the phonon intensity tends to zero. This coincides with the fact that the rays associated with an infinitesimal neighborhood of the conical point are distributed over a finite elliptical cone (or circular if the conical point lies on an axis of threefold symmetry). This ellipse or circle of zero phonon intensity is called an anticaustic.

The lifting of the degeneracy at finite ω or k causes the two sheets of the slowness surface to become separated and rounded off as depicted by the dashed or dotted curves in Fig. 1(a). The outer ST sheet now possesses a small concave region which is bounded by a parabolic line passing through the inflection points 1 and 2 (or 1′ and 2′). This results in the formation of a caustic which replaces the original anticaustic. Initially this caustic is very faint. With increasing ω the splitting of the two sheets widens and the parabolic line expands outwards (as depicted by the movement of the inflection points from 1 to 1′ and 2 to 2′). This causes the caustic to grow more intense and contract inwards (note how the rays at 1′ and 2′ are more nearly parallel). Figure 1(b) shows a phonon intensity pattern for $NaBrO_3$ (crystal class 23) in the vicinity of the ⟨111⟩ acoustic axis, taking $d'_{543}k/C_{44}=0.0022$ (the prime indicates transformed axes with $\mathbf{X}_3\|\langle 111\rangle$). The position of the original circular anticaustic is shown by the dashed circle. The caustic which has evolved from it, and which is labeled A, is no longer perfectly circular. The much more intense caustics labeled B are present for $\omega,k,\rightarrow 0$ and are not significantly affected by dispersion.

In order to experimentally follow the evolution of caustic A one would need to employ either a monochromatic source of phonons or else precise wave-vector selection, exacting demands which are not easily met in practice.

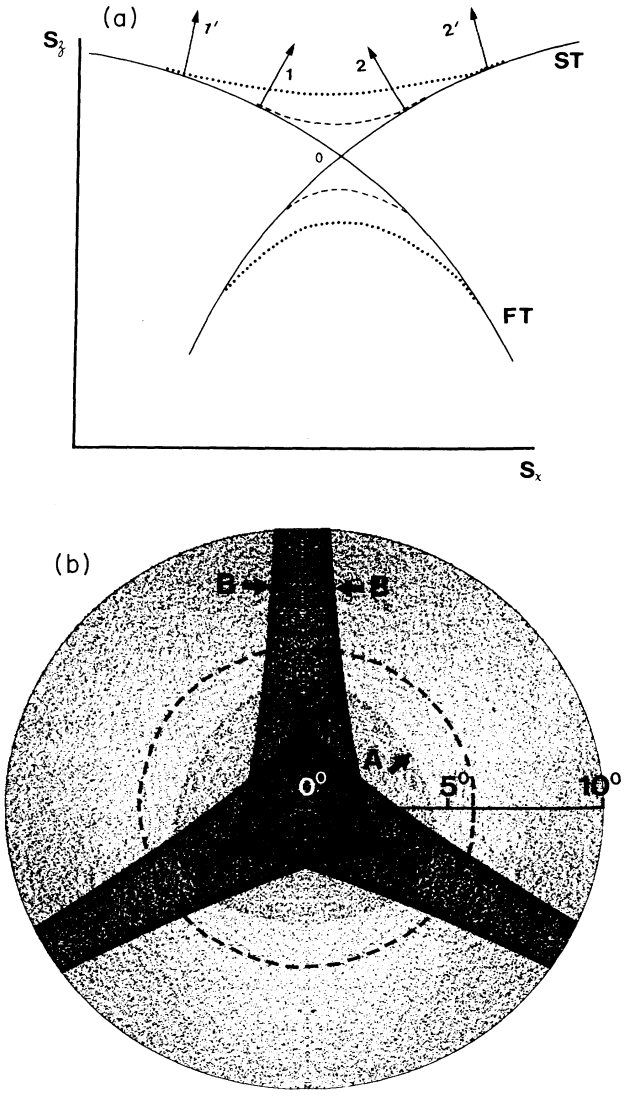

FIG. 1. (a) Schematic section through a slowness surface showing the meeting of the T sheets at a conical point (solid curves). At finite frequency the two sheets are separated as shown by the dashed curves (small k or ω) or dotted curves (larger k or ω). (b) ST and FT polar phonon intensity pattern for $NaBrO_3$ centered on the ⟨111⟩ acoustic axis (C_{11}:C_{12}:$C_{44}=3.66$:1.18:1, $d'_{543}k/C_{44}=0.0022$). Darkness of the grey scale denotes the phonon intensity. Dashed line indicates the circle of conical refraction.

Under more realistic conditions the observed phonon focusing pattern will be a superposition of a continuous distribution of constant-frequency focusing patterns. The result of this will be a focusing pattern in which the phonon intensity builds up smoothly from the circle inwards.

A more complex situation arises where there are parabolic lines which penetrate through a conical point from one slowness sheet to the other. A large class of cubic crystals display this phenomenon[29-31] and it is also common in trigonal crystals.[30] This produces caustics that meet the anticaustic tangentially, fading in intensity to zero as they do so. The discussion of how these caustics evolve at finite k is deferred to Sec. IV A, where focusing in the region of the c axis of quartz is treated.

In directions of fourfold and sixfold symmetry the transverse sheets of the $\omega \rightarrow 0$ slowness surface meet tangentially. The curvature of both sheets remains finite in the vicinity of the point of contact (although the curvature at the point of contact is undefined), and so an anticaustic does not develop here. In the case of a fourfold axis, for certain ranges of elastic constants there can be sets of symmetry equivalent parabolic lines on either or both the T sheets which pass through their point of contact. This gives rise to sets of intersecting line caustics, a common feature in many cubic crystals. At finite ω the gyrotropic coupling causes the two sheets of the slowness surface to come apart and the parabolic lines join up in pairs without reaching the fourfold axis. Figure 2 shows a polar phonon intensity pattern for $NaClO_3$, taking $d_{543}k/C_{44}=0.0043$. Dashed lines indicate the location of the caustics for $\omega \rightarrow 0$. For finite ω these caustics terminate in cusps before reaching the cube axis.

A third form of degeneracy takes the form of two sheets of the slowness surface intersecting along a line.[30,34] These lines of wedge-shaped degeneracy are quite common in hexagonal crystals, where they derive their structural stability from the transverse elastic isotropy. They also occur in cubic and other crystals for special values of the elastic constants.[30] For the crystal classes $\bar{6}$ and $\bar{6}m2$ piezoelectric stiffening of the elastic constants removes this line degeneracy, leaving in its place a finite set of points of conical degeneracy.[35] In the other noncentrosymmetric hexagonal classes this line degeneracy is lifted at finite k by acoustic gyrotropy. All the nonvanishing components of d_{IJn} need to be taken into account in order to properly determine the changes to the transverse velocities and how the lifting of the degeneracy varies with direction. We will consider as a specific example, the special case where $d_{543}\neq 0$, while all other inequivalent components of d_{IJn} are zero. This preserves the transverse isotropy but lifts the degeneracy uniformly over the entire circles where the transverse sheets of the slowness surface intersect at $k=0$. This results in bands of elliptical acoustic birefringence centered on the original circles of intersection. Pairs of circular caustics develop in a manner analogous to the global formation of caustics when a trigonal distortion lifts this degeneracy.[30] In the latter case, however, there is a threefold pattern of cusps which is not present here. Figure 3 shows a polar phonon intensity plot for a hypothetical hexagonal medium with $d_{543}k/C_{44}=0.1$. The circular caustics referred to above are labeled A and B.

IV. PHONON FOCUSING IN QUARTZ

Quartz has featured prominently in investigations of first-order spatial dispersion,[16,18-22] phonon focusing,[11,12,36] and ballistic heat pulse propagation.[10] Detailed

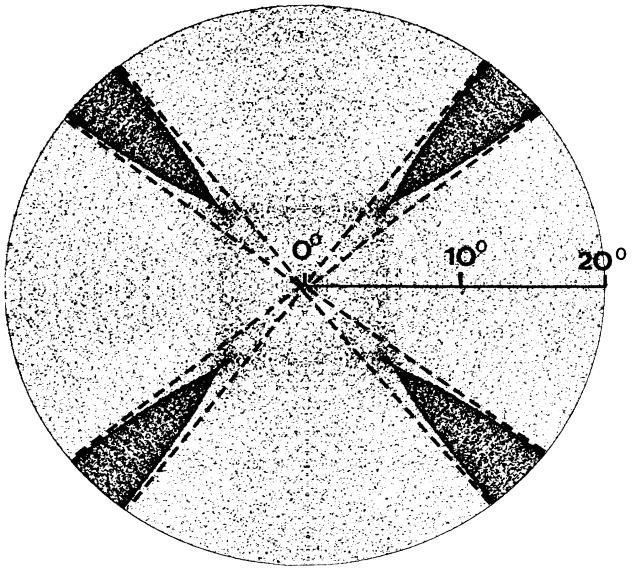

FIG. 2. ST and FT polar phonon intensity pattern for $NaClO_3$ centered on the $\langle 100 \rangle$ acoustic axis (C_{11}:C_{12}:C_{44} $=4.28$:1.27:1, $d_{543}k/C_{44}=0.0043$). Dashed lines indicate the caustics for $k \rightarrow 0$.

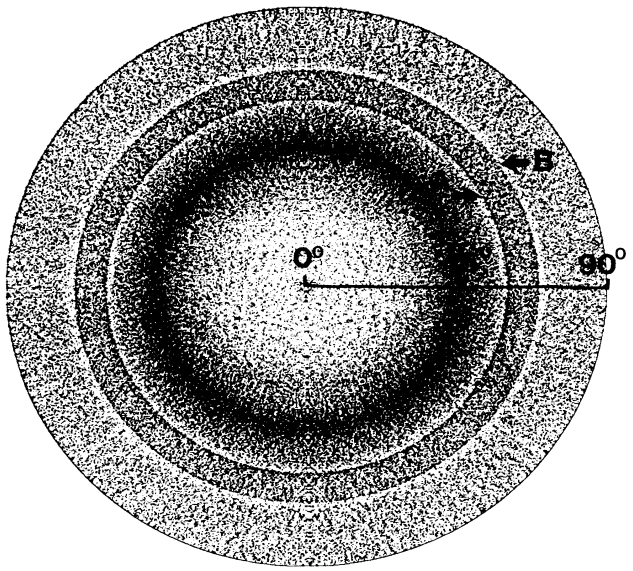

FIG. 3. ST and FT polar phonon intensity pattern for a hypothetical hexagonal medium with C_{11}:C_{33}:C_{12}:C_{13}:C_{44} $=4$:4:1.8:1.6:1 and $d_{543}k/C_{44}=0.1$.

phonon focusing patterns were first predicted for α quartz by Rösch and Weis.[36] Overall, their predictions have been borne out in the experimental phonon images of Eichele *et al.*[12] and Koos and Wolfe.[11] However, the latter authors, who will hereafter be referred to as KW, pointed out some striking anomalies in their phonon images which could not be reconciled with theory, even allowing for quite substantial adjustments to the low-frequency elastic constants. It is noteworthy that these anomalies all occur in the vicinity of the conical points of quartz. We show below that first-order spatial dispersion is well able to explain a number of these anomalies.

The crystal point group of α quartz is 32, which allows eight independent components for d_{IJn}.[15] Only three of these are, however, accessible to dynamical measurement[37] and, in the event, only d_{543} has actually been experimentally determined. The reason for this is that in the past studies of acoustic gyrotropy in quartz have been confined to the conic point lying on the c axis. At finite frequency ν, the relative splitting between the phase velocities of left and right circularly polarized modes propagating along this axis is given by[21]

$$\frac{v_+ - v_-}{\bar{v}} = \gamma\nu \ , \tag{9}$$

where $\gamma = 2\pi d_{543}/C_{44}\bar{v}$, is the gyrotropic constant. γ has been determined by various methods,[18,20–22] and the published values range from $(2.8–3.7)\times 10^{-4}$ GHz^{-1}. In our calculations we have taken $\gamma = 3.0\times 10^{-4}$ GHz^{-1}, a value decided on after consideration of the reported accuracies of the various experimental techniques. We have used the same values for the elastic constants, piezoelectric stress coefficients, permittivity, and density as have KW (Ref. 11) in their calculations. From these values one obtains $\bar{v} = (C_{44}/\rho)^{1/2} = 4726$ m/s and $d_{543} = 13.4$ N/m. The electromechanical coupling in quartz is small, and we find that the inclusion of piezoelectric stiffening of the elastic constants has a negligible effect on our results, even with dispersion included.

Jouffroy and Levinson[10] have invoked the idea of first-order spatial dispersion to explain their heat pulse results in quartz. They confine their attention, however, to three specific directions near the c axis and develop their analysis in the approximation that there is cylindrical symmetry around the c axis. Our treatment goes beyond this approximation and explores the detailed evolution of the phonon focusing pattern with dispersion. We also examine the effects of acoustic gyrotropy on the other conical points, a topic which has not been broached before.

A. Phonon focusing caustics near to c axis

Figure 4(a) depicts the limiting low-frequency ST and FT caustics and circular anticaustic in the region of the c axis of quartz. The six-cusped triangular-shaped structure, labeled E, is the unfolded form of the external conical refraction caustic that emerges with reduction from hexagonal (transverse isotropy) to trigonal symmetry.[30] The pattern of alternating ST and FT caustics, labeled S and F, that touch the circular anticaustic at six points is mapped from a parabolic line that weaves back and forth

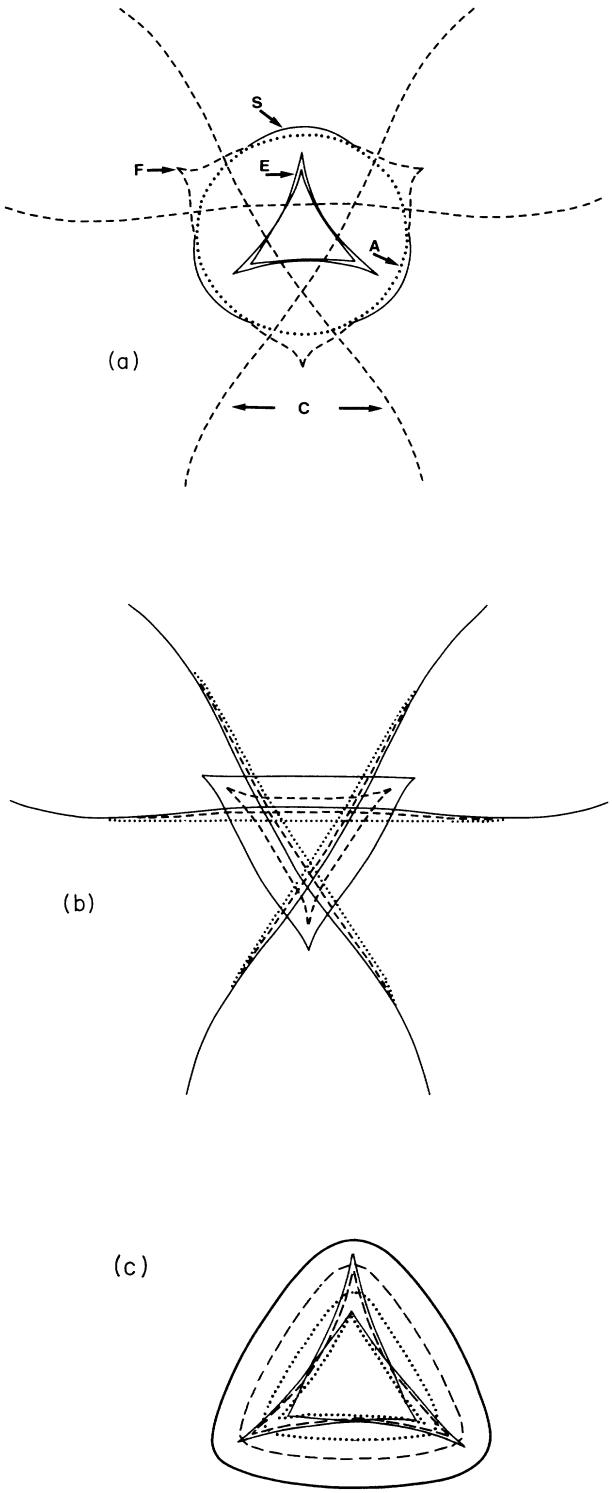

FIG. 4. (a) Circular anticaustic (· · · ·), ST caustics (——), and FT caustics (— — —) near the c axis of quartz in the limit $k,\nu\to 0$. (b) Evolution of the FT caustics with increasing k: ——, $k = 2\times 10^8$ m^{-1} ($\nu\sim 150$ GHz); — — —, $k = 4\times 10^8$ m^{-1} ($\nu\sim 300$ GHz); and · · · ·, $k = 6\times 10^8$ m^{-1} ($\nu\sim 450$ GHz). (c) Evolution of the ST caustics with k.

through the conical point. This line separates alternating regions of positive and negative Gaussian curvature of the slowness surface surrounding the conical point. The three fairly-straight-line cautics, labeled C, are due to parabolic lines on the FT slowness sheet which pass fairly close to the conical point.

Figure 4(b) shows the evolution of the FT caustics and Fig. 4(c) that of ST caustics as k is increased and the two sheets of the slowness surface move apart. Immediately dispersion is introduced, the separated segments F of the FT caustic become joined together by very faint connecting-line caustics that follow the path of the original anticaustic, and the ST caustics S undergo a similar transformation. As k increases further, the faint connecting portions of S and F contract rapidly inwards, growing in intensity as they do so, while the original segments move inwards more slowly so that both these caustics become roughly triangular in shape. With further increase in k both caustics continue to contract inwards and eventually become enmeshed with the intense caustic E.

Because of the rapid contraction of the caustics F and S with increasing k, when the phonon intensity patterns for a distribution of k's are superposed, F and S do not survive as singular features. The main result of the superposition is a gradual buildup in phonon intensity towards the central region near the c axis. The retreating FT cusps deposit an especially large concentration of phonon intensity in their wake, and integration over a broad distribution of k's yields the intense three-spoked structure located at the center of Fig. 5(a). This structure matches up well with an hitherto unexplained feature in the early time (800 ns) phonon image of quartz reported by KW [their Fig. 5(a)]. The main contribution to this structure arises from modes with $k > 2\times 10^8$ m^{-1} which have frequencies $\nu > 150$ GHz, and group-velocity components $V_3 > 4900$ m/s. For k's in excess of 2×10^8 m^{-1}, the lifting of the degeneracy reduces V_3 for the ST modes to below 4500 m/s. The increased separation between ST and FT mode velocities helps to explain why the three-spoked structure is such a prominent feature of the early-time image KW [Fig. 5(a)], but is almost totally absent from the later-time images KW [Figs. 5(c) and 5(d)]. Moreover, there is no sign of the ST focusing structures in the early time image.

With increasing k the three FT line caustics C undergo lateral displacements which bring their points of intersection inwards towards the c axis. The displacement is least at the extremities of the lines and greatest near the center. These shifted central portions are, moreover, composed of FT phonons which have had their velocities increases by the lifting of the degeneracy. The consequences of this are evident in the early-time image KW [Fig. 5(a)] in the form of a progressive blurring of the FT line caustics towards the center. In the later-time images, KW [Figs. 5(b) and 5(c)], which one would expect to give greater weight to lower-velocity smaller **k** phonons, the blurring is much less, and the FT caustics have their predicted low-frequency shape.

With increasing k the ST structure E contracts gradually inwards, retaining is shape essentially unchanged. This structure is composed of phonons with velocities in the range $4000 < V_3 < 4500$ m/s and therefore, as expected, it shows up most prominently in the medium- and later-time images KW [Figs. 5(b) and 5(c)]. These images are composed of lower-velocity phonons as well as a proportion of higher-velocity phonons which have been delayed before emission. The effects of dispersion are therefore to a large extent masked and thus more difficult to recognize, as compared with the early-time images. The 1100-ns experimental image KW [Fig. 5(d)] is dominated by six short bright segments of ST precursors. These structures are composed of phonons with k's lying far from the

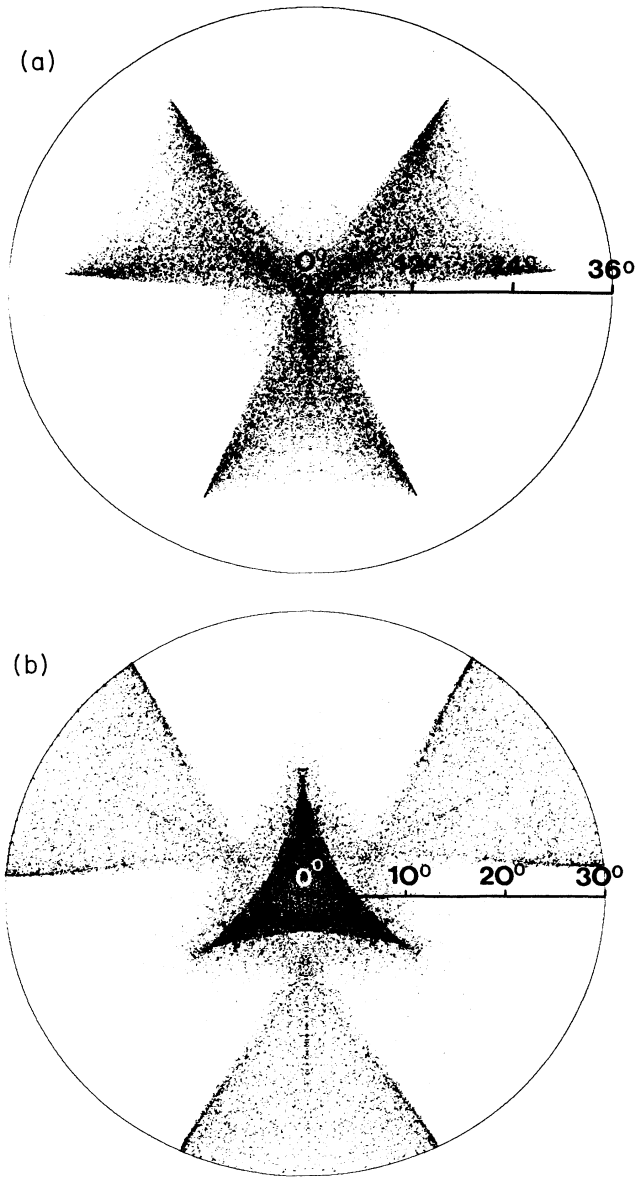

FIG. 5. (a) Polar phonon intensity pattern for quartz restricted to transverse modes with $V_3 > 4800$ m/s. The phonon temperature is $T = 10$ K, $d_{543} = 13.4$ N/m, and $k_{max} = 1.162\times 10^9$ m^{-1}. (b) Corresponding pattern for the transverse modes with $V_3 > 4000$ m/s and $T = 3.3$ K.

acoustic axis, and are well accounted for without invoking dispersion.

B. Monte Carlo simulation of phonon intensity near to c axis

The qualitative points made in Sec. IV A are confirmed by Monte Carlo simulations of the temperature-dependent phonon focusing pattern of quartz. We assume that a Planck distribution of phonons is emitted from the heat source. The spectral energy distribution of these phonons peaks at $\nu \sim 2.8 k_B T/h$, and has a tail extending to higher frequencies. One has also to consider the effects of phonon scattering. In general, depending on the precise mechanism, the rate of scattering increases rapidly with frequency (e.g., isotope and point defect scattering as ν^4, etc.). The result of this is that towards 1 THz and beyond there is a rapid falloff in the proportion of phonons that maintain ballistic trajectories through the crystal and arrive within the time gates of the detector.

In our calculations we have assumed a sharp cutoff for ballistic propagation, restricting acoustic phonon wave vectors to a sphere of radius $k_{\max} = 0.1 k_{\mathrm{BZ}} = \frac{1}{10} \times 2\pi/c = 1.162 \times 10^9\ \mathrm{m}^{-1}$, where $c = 5.404$ Å is the c-axis cell dimension. This cutoff corresponds to a maximum phonon frequency $\nu_{\max} = k_{\max} v/2\pi \simeq 0.9$ THz. Having this cutoff also serves another important purpose: The neutron scattering results of Joffrin *et al.*[16] indicate that at about $k = 0.1 k_{\mathrm{BZ}}$ the slope of the FT dispersion curve $(= \partial\omega/\partial k_3 = V_3)$ reaches a maximum whereafter the curve bends over and levels off. This effect arises from higher-order terms in the expansion of $C_{ijlm}(\mathbf{k})$ which we have not built into our calculations. Interestingly, clear evidence for the existence of this maximum in the phonon group velocity is provided by the heat-pulse experiments of Jouffroy and Levinson.[10] Assuming a heat source temperature of 10 K, which is fairly typical in phonon imaging,[38] the peak in the phonon spectral energy distribution occurs at $\nu \sim 0.58$ THz. This is sufficiently far below the cutoff frequency that the precise position assumed for the cutoff does not drastically affect the final results.

Our Monte Carlo image construction process consists in generating a uniform random distribution of $\mathbf{k}$'s within the cutoff sphere and solving the wave equation to obtain the frequencies and group velocities of the modes belonging to each value of $\mathbf{k}$. Each mode is then given a weighting proportional to $\bar{n}\hbar\omega = \hbar\omega[\exp(\hbar\omega/k_B T) - 1]^{-1}$, and the weighted ray vectors are sorted in direction to form a polar plot of the phonon intensity.

Figure 5(a) shows a polar phonon-intensity diagram for quartz, restricted to transverse modes with group-velocity components $V_3 \geq 4800$ m/s. This intensity pattern is in good agreement with the phonon image of KW [Fig. 5(a)] obtained with an early (800 ns) setting of the time gates. The three-spoked structure at the center, and the progressive blurring of the FT line caustics towards the center match up well with corresponding features in the experimental image. Since the average value of V_3 for the modes in this diagram is ~ 5000 m/s one infers that the thickness of the sample used by KW was $l = 5000$ m/s $\times$ 800 ns $= 4$ mm, whereas KW have actually given the value as 3 mm.

When the cutoff is set at $k_{\max} = \frac{1}{15} \times 2\pi/c$, which corresponds to a frequency cutoff $\nu_{\max} \simeq 0.6$ THz, the central region of the three-spoked structure all but disappears, and the blurring of the FT line caustics is considerably reduced. Similar changes take place when the heat-source temperature is lowered appreciably. In both cases agreement with the 800-ns image is no longer nearly as good. One concludes from this that a significant proportion of acoustic phonons in the frequency range $0.6 < \nu < 0.9$ THz have been able to propagate ballistically under the experimental conditions, and secondly that the heat-pulse temperature in the experiment of KW could not have been much less than ~ 10 K. It would be of interest to see whether the detailed predictions of this model for the effects of changing temperature could be verified experimentally by varying, for example, the laser excitation intensity in a phonon imaging experiment.

The abnormal dispersion of the FT branch also provides a means for frequency filtering to obtain phonons in the spectral range ~ 0.6–0.9 THz. The inner portions of the three-spoked structure, as we see have seen, are composed almost entirely of these phonons.

In the phonon images of KW [Figs. 5(b) and 5(c)] obtained with later settings of the time gates, the caustics are much sharper than before, and they conform more closely to their predicted low-frequency limiting shape. Evidently therefore these images are composed of a much narrower spectrum of phonons which have been delayed and emitted during the cooling cycle of the metal heater film. On assuming an effective phonon temperature of 3.3 K at this stage, we obtain the polar phonon intensity plot shown in Fig. 5(b). It is in reasonably good agreement with KW [Fig. 5(b)]. This does not remain so if the temperature is taken much higher or lower than 3.3 K.

C. Phonon focusing near to nonsymmetry acoustic axes

There are also significant discrepancies between the experimental and predicted low-frequency phonon focusing patterns of quartz in the general vicinity of the direction $(\theta = 65°, \phi = 30°)$. There are three acoustic axes located in this region, which lie along the directions (65.50°, 30°), (64.28°, 36.89°), and (64.28°, 23.11°). These are not high-symmetry directions and so the conical points are of the elliptical variety. Experimental investigations of first-order spatial dispersion and acoustical activity in the past have been restricted exclusively to acoustic axes lying in directions of threefold and fourfold symmetry. It is doubtless that the added practical difficulties of applying the existing techniques where there is not the advantage of symmetry has been a major deterring factor. Phonon imaging, on the other hand, does not suffer from this drawback and should yield information on nonsymmetry conical points just as readily as for those along symmetry axes.

The theoretical interpretation of first-order spatial dispersion at nonsymmetry concial points is complicated by the involvement of all three matrix elements $\Gamma_{12}^{(1)}$, $\Gamma_{23}^{(1)}$, and $\Gamma_{31}^{(1)}$. Considerable simplification is, however, gained by orienting the X_3 axis along the polarization direction for the isonormal longitudinal mode. In this case the lift-

ing of the degeneracy is effected by Γ_{12} alone, and for $\mathbf{k}$ close to the X_3 direction $\Gamma_{12}^{(1)}=d_{543}k_3^3$. Thus, as before, there is only one component of the gyrotropic tensor to consider. Figure 6(a) shows the limiting $k\rightarrow 0$ phonon intensity pattern for quartz in the vicinity of the direction (65.5°, 30°). The three nonsymmetry conical points mentioned above and their elliptical anticaustics all fall in the field of view. Since these three conical points are fairly close together, we have assumed that rotating the X_3 axis into the direction (65.5°, 30°) and adopting just a single dispersion term $\Gamma_{12}^{(1)}=-\Gamma_{21}^{(1)}=id'_{543}k_3^3$ provides an adequate approximation to the different terms that cause the lifting of the degeneracy of each of the three conical points. Figure 6(b) shows the phonon intensity pattern obtained by taking $d'_{543}=d_{543}=13.4$ N/m, $k_{\max}=0.1\times 2\pi/c$, and $T=10$ K. A considerable blurring of the focusing structures occurs as a result of dispersion.

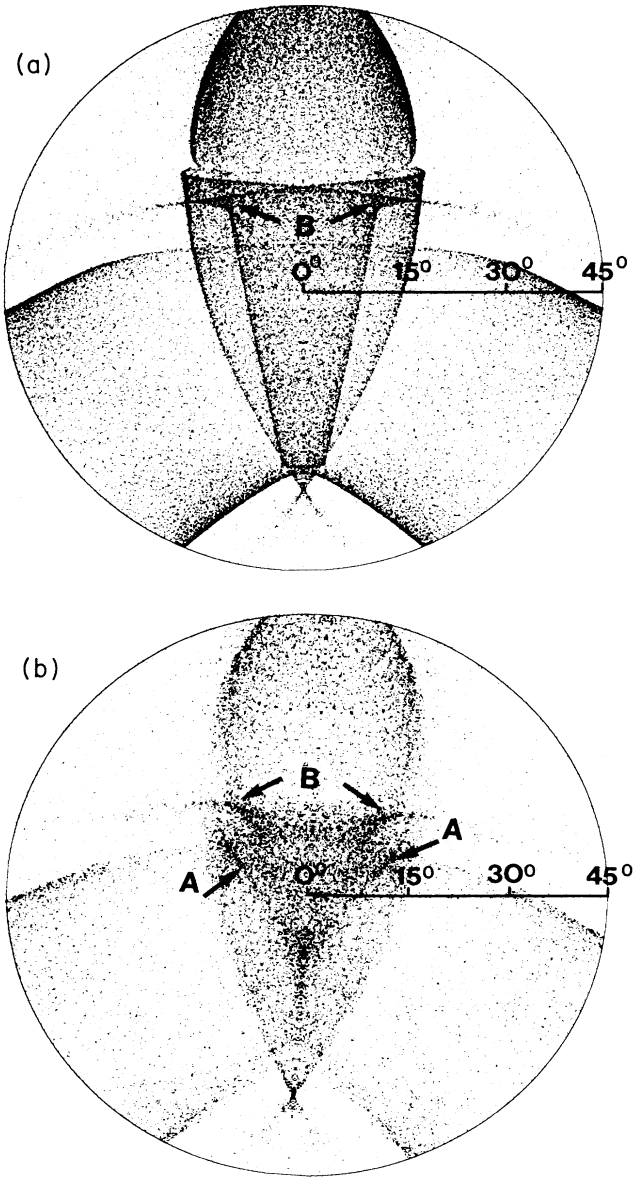

FIG. 6. ST and FT phonon intensity pattern for quartz centered on the direction ($\theta=65.5°$, $\phi=30°$). (a) In the $k\rightarrow 0$ limit. (b) For $T=10$ K, $d'_{543}=13.4$ N/m and $k_{\max}=1.162\times 10^9$ m^{-1}, with no restriction on the velocities of the modes.

The experimental image obtained by KW (Fig. 6) for their Y-cut specimen actually bears closer resemblance to the theoretical $k\rightarrow 0$ focusing pattern, particularly in regard to the sharpness of the caustics. This could imply that d'_{543} is much smaller than d_{543}. The correct interpretation must, however, take into account the extremely wide time gate (800 ns) used in recording the experimental image. Much greater weighting has thereby been given to phonons emitted during the cooling cycle of the heat film, and so the effective temperature for that image is much less than 10 K.

An important feature not accounted for by the low-frequency simulation is a diffuse V-shaped structure near the center of the experimental image. This bears some resemblance to the structure marked A in Fig. 6(b) and so could be a relic of the focusing of higher-temperature phonons. The sharp-cusped structure labeled B which is present in both theoretical phonon intensity plots is unaccountably absent from the experimental image.

Narrow time-gated phonon imaging on quartz samples with faces cut at an angle to the c axis would be of great value in helping to resolve these points.

V. CONCLUSIONS

First-order spatial dispersion has been shown to account for a number of anomalies in the phonon focusing pattern of quartz. Even at the relatively low frequencies encountered in conventional phonon imaging based on bolometric detection techniques, there are pronounced changes to the focusing pattern near to the acoustic axes.

Phonon imaging is placed in an advantageous position to probe spatial dispersion at nonsymmetry acoustic axes. Although the agreement between our calculations and experiment for such axes in quartz is less than satisfactory, time-resolved imaging is needed before a proper comparison can be made.

The absence of a center of inversion is a prerequisite for first-order spatial dispersion.[39] Since most of the crystals subjected to phonon imaging in the past have been centrosymmetric, this would explain why the influence of spatial dispersion on phonon focusing has not been widely appreciated before now. However, as more noncentrosymmetric crystals come to be examined dispersion is likely to become an important consideration.

Useful returns that could emerge from a study of the effects of first-order spatial dispersion on phonon focusing are practical means for measuring phonon temperatures and for frequency filtering of thermal phonons.

ACKNOWLEDGMENTS

The author would like to thank M. J. Hoch for providing access to computing facilities. He has benefitted during the formative period of the ideas presented here from discussions with J. P. Wolfe, G. A. Northrop, H. J. Maris, and D. P. DiVincenzo.

[1]For recent reviews on phonon focusing and phonon imaging, see H. J. Maris, in *Nonequilibrium Phonons in Nonmetallic Crystals,* edited by W. Eisenmenger and A. A. Kaplyanskii (North-Holland, Amsterdam, 1986), p. 51; G. A. Northrop and J. P. Wolfe, in *Nonequilibrium Phonon Dynamics,* edited by W. E. Bron (Plenum, New York, 1985), p. 165.

[2]R. G. Ulbrich, V. Narayanamurti, and M. A. Chin, Phys. Rev. Lett. **45**, 1432 (1980).

[3]W. Dietsche, G. A. Northrop, and J. P. Wolfe, Phys. Rev. Lett. **47**, 660 (1981); G. A. Northrop, Phys. Rev. B **26**, 903 (1982).

[4]G. A. Northrop, S. E. Hebboul, and J. P. Wolfe, Phys. Rev. Lett. **55**, 95 (1985).

[5]S. E. Hebboul and J. P. Wolfe, Phys. Rev. B **34**, 3948 (1986).

[6]S. Tamura and T. Harada, Phys. Rev. B **32**, 5245 (1985); S. Tamura, *ibid.* **28**, 897 (1983); K. Okubo and S. Tamura; *ibid.* **28**, 4847 (1983).

[7]D. L. Portigal and E. Burstein, Phys. Rev. **170**, 673 (1968).

[8]G. Kluge, Phys. Status Solidi **17**, 109 (1966).

[9]D. P. DiVincenzo, Phys. Rev. B **34**, 5450 (1986).

[10]J. Jouffroy and P. Levinson, J. Phys. (Paris) **36**, 709 (1975).

[11]G. L. Koos and J. P. Wolfe, Phys. Rev. B **30**, 3470 (1984).

[12]R. Eichele, R. P. Huebener, H. Seifert, and K. P. Selig, Phys. Lett. **87A**, 469 (1982); R. Eichele, R. P. Huebener, and H. Seifert, Z. Phys. B **48**, 89 (1982).

[13]B. A. Auld, *Acoustic Fields and Waves in Solids* (Wiley, New York, 1973).

[14]J. F. Nye, *Physical Properties of Crystals* (Oxford University Press, London, 1969).

[15]K. Kumaraswamy and N. Krishnamurthy, Acta Crystallogr. Sect. A **36**, 760 (1980).

[16]C. Joffrin, B. Dorner, and J. Joffrin, J. Phys. (Paris) Lett. **41**, L391 (1980).

[17]C. Lin, T. Fang, Z. Tai-yong, N. Shi-wen, G. Cheng, and S. Zhong-jian, Solid State Commun. **54**, 803 (1985).

[18]A. S. Pine, J. Acoust. Soc. Am. **49**, 1026 (1971).

[19]A. S. Pine, Phys. Rev. B **2**, 2049 (1970).

[20]J. Joffrin and A. Levelut, Solid State Commun. **8**, 1573 (1970).

[21]H. Bialas and G. Schauer, Phys. Status Solidi A **72**, 679 (1982).

[22]M. F. Bryzhina, S. Kh. Esayan, and V. V. Lemanov, Pis'ma Zh. Eksp. Teor. Fiz. **25**, 513 (1977) [JETP Lett. **25**, 483 (1977)]; M. F. Bryzhina and S. Kh. Esayan, Fiz. Tverd. Tela **20**, 2628 (1978) [Sov. Phys.—Solid State **20**, 1519 (1978)].

[23]M. J. P. Musgrave, Proc. R. Soc. (London), Ser. A **401**, 131 (1985).

[24]A. G. Every, Phys. Rev. B **22**, 1746 (1980).

[25]A. G. Every and A. K. McCurdy, Phys. Rev. B **36**, 1432 (1987).

[26]H. J. Maris, J. Acoust. Soc. Am. **50**, 812 (1971).

[27]G. A. Northrop and J. P. Wolfe, Phys. Rev. B **22**, 6196 (1980).

[28]M. Lax, and V. Narayanamurti, Phys. Rev. B **22**, 4876 (1980).

[29]A. G. Every, Phys. Rev. B **24**, 3456 (1981).

[30]A. G. Every, Phys. Rev. B **34**, 2852 (1986).

[31]D. C. Hurley and J. P. Wolfe, Phys. Rev. B **32**, 2568 (1985).

[32]D. Armbruster and G. Dangelmayr, Z. Phys. B **52**, 87 (1983).

[33]W. Dietsche, in *Phonon Scattering in Condensed Matter V,* Vol. 68 of *Springer Series in Solid State Sciences,* edited by A. C. Anderson and J. P. Wolfe, (Springer-Verlag, Berlin, 1986), p. 366.

[34]V. I. Al'shits, A. V. Sarychev, and A. L. Shuvalov, Zh. Eksp. Teor. Fiz. **89**, 922 (1985) [Sov. Phys.—JETP **62**, 531 (1985)].

[35]A. G. Every, J. Phys. C (to be published).

[36]F. Rösch and O. Weis, Z. Phys. B **25**, 101 (1976).

[37]A. D. Vuzhva and V. E. Lyamov, Kristallografiya **22**, 131 (1977) [Sov. Phys.—Crystallogr. **22**, 73 (1977)].

[38]A. G. Every, G. L. Koos, and J. P. Wolfe, Phys. Rev. B **29**, 2190 (1984).

[39]Acoustic activity is also absent for the crystal class $\bar{4}3m$. See Ref. 7.